Available online at www.sciencedirect.com
SCIENCE DIRECT®
Journal of Solid State Chemistry 178 (2005) 2741–2750
JOURNAL OF SOLID STATE CHEMISTRY
www.elsevier.com/locate/jssc

Lithium ion insertion and extraction reactions with Hollandite-type manganese dioxide free from any stabilizing cations in its tunnel cavity

Norihito Kijima*, Yasuhiko Takahashi, Junji Akimoto, Junji Awaka

National Institute of Advanced Industrial Science and Technology (AIST), Tsukuba Central 5, 1-1-1 Higashi, Tsukuba, Ibaraki 305-8565, Japan

Received 1 April 2005; received in revised form 28 May 2005; accepted 6 June 2005
Available online 26 July 2005

Abstract

Lithium ion insertion and extraction reactions with a hollandite-type α-MnO_2 specimen free from any stabilizing cations in its tunnel cavity were investigated, and the crystal structure of a Li^+-inserted α-MnO_2 specimen was analyzed by Rietveld refinement and whole-pattern fitting based on the maximum-entropy method (MEM). The pH titration curve of the α-MnO_2 specimen displayed a monobasic acid behavior toward Li^+, and an ion-exchange capacity of 3.25 meq/g was achieved at pH > 11. The Li/Mn molar ratio of the Li^+-inserted α-MnO_2 specimen showed that about two Li^+ ions can be chemically inserted into one unit cell of the hollandite-type structure. As the amount of Li content was increased, the lattice parameter a increased while c hardly changed. On the other hand, the mean oxidation number of Mn decreased slightly regardless of Li content whenever ions were exchanged. The Li^+-inserted α-MnO_2 specimen reduced topotactically in one phase when it was used as an active cathode material in a liquid organic electrolyte (1:1 EC:DMC, 1 mol/dm^3 $LiPF_6$) lithium cell. An initial discharge with a capacity of approximately 230 mAh/g was achieved, and the reaction was reversible, whereas the capacity fell steadily upon cycling. About six Li^+ ions could be electrochemically inserted into one unit cell of the hollandite-type structure. By contrast, the parent α-MnO_2 specimen showed a poor discharge property although no cationic residues or residual H_2O molecules remained in the tunnel space. Rietveld refinement from X-ray powder diffraction data for a Li^+-inserted specimen of $(Li_2O)_{0.12}MnO_2$ showed it to have the hollandite-type structure (tetragonal; space group $I4/m$; $a = 9.993(11)$ and $c = 2.853(3)$ Å; $Z = 8$; $R_{wp} = 6.12\%$, $R_p = 4.51\%$, $R_B = 1.41\%$, and $R_F = 0.79\%$; $S = 1.69$). The electron-density distribution images in $(Li_2O)_{0.12}MnO_2$ showed that Li_2O molecules almost fill the tunnel space. These findings suggest that the presence of stabilizing atoms or molecules within the tunnel of a hollandite-type structure is necessary to facilitate the diffusion of Li^+ ions during cycling.

Keywords: α-MnO_2; Hollandite-type structure; X-ray powder diffraction; Rietveld analysis; Maximum-entropy method; Electron-density distribution; Ion-exchange property; Charge–discharge property

1. Introduction

Several manganese oxides with tunnel structures have been synthesized so far [1–5]. α-MnO_2 has a hollandite-type structure (space group $I4/m$, No. 87) comprising double chains of MnO_6 octahedra forming (2×2) tunnels, as shown in Fig. 1. At present, only α-MnO_2 is known to have a tunnel structure without any large stabilizing cations in its tunnel cavity, whereas the other porous manganese oxides, e.g., romanechite (2×3) and todorokite (3×3), contain some large stabilizing cations in their tunnels. The open-tunnel structure of α-MnO_2 makes it attractive for various industrial applications such as an electrode material for lithium-ion secondary batteries [2,6–19] and an ion- or molecular-sieve [4,20–26].

Various methods have been used to prepare α-MnO_2, with different influences on the properties of the products. Most α-MnO_2 samples include cationic

*Corresponding author.
E-mail address: n-kijima@aist.go.jp (N. Kijima).

0022-4596/$ - see front matter © 2005 Elsevier Inc. All rights reserved.
doi:10.1016/j.jssc.2005.06.023

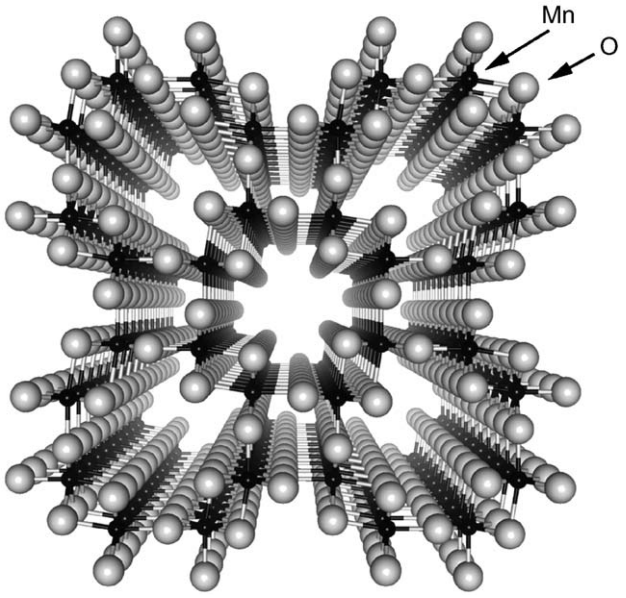

Fig. 1. Schematic drawing of the crystal structure of α-MnO_2 of a hollandite-type structure with space group of $I4/m$ (No. 87). The crystal structure is viewed along the c-axis.

residues such as Li^+, K^+, and Ba^{2+} ions in their tunnels because precursors containing such cations are usually used in their synthesis. These residual cations would impede the diffusion of Li^+ ions in the tunnels during electrochemical operation and also reduce the material's ion-exchange capacity. Presumably, if an α-MnO_2 specimen free from any cationic residues could be synthesized, its properties would be improved significantly.

We have recently succeeded in synthesizing a high-purity and well-crystallized specimen of α-MnO_2 free from any stabilizing cations in its tunnel cavity by a precipitation method using ozone oxidation [27,28]. Using our synthetic method, α-MnO_2 can directly be formed in solutions containing no cations other than Mn^{2+}. Therefore, a high-purity specimen free from any cationic residues in the tunnels can be obtained.

In this work, we investigated ion-exchange and electrochemical properties of the α-MnO_2 specimen free from stabilizing cations in its tunnel cavity. To clarify the structural properties of a Li^+-inserted α-MnO_2 specimen, we also refined its structure parameters by Rietveld analysis from X-ray powder diffraction data. Furthermore, we visualized electron-density distribution (EDD) in the Li^+-inserted α-MnO_2 specimen by whole-pattern fitting (w.p.f.) based on the maximum-entropy method (MEM) [29–31]. EDD determined in this way is expected to provide valuable information on the residual atoms or molecules in the tunnel cavity.

Contrary to our expectation, the parent α-MnO_2 specimen showed a poor discharge property although no cationic residues and residual H_2O molecules remained in the tunnel space. In contrast, the Li^+-inserted α-MnO_2 specimen exhibited a good charge–discharge property as the cathode. The EDD images in the Li^+-inserted specimen showed that Li_2O molecules occupy the tunnel space almost entirely. These facts suggest that the presence of stabilizing atoms or molecules within the (2×2) tunnel of the hollandite-type structure is necessary to facilitate the diffusion of Li^+ ions during cycling. We discuss here both electrochemical and chemical lithium ion insertion/extraction reactions with hollandite-type MnO_2 (HMO).

2. Experimental

2.1. Sample preparation

An α-MnO_2 specimen was prepared by the precipitation method using ozone oxidation [27,28]. Scanning electron microscopy (SEM) images of the α-MnO_2 specimen showed that the surfaces of particles were covered almost uniformly with needle-like crystals, which were elongated parallelly to the c-axis, i.e., along the direction of the tunnel (Fig. 2). Details of the preparation and characterization of α-MnO_2 have been reported in previous works [27,28].

A Li^+-inserted α-MnO_2 specimen was obtained by soaking the parent α-MnO_2 powder in a mixed solution of 0.1 mol/dm^3 LiOH and 0.1 mol/dm^3 $LiNO_3$ at a 1:1 volumetric ratio. Five grams of the α-MnO_2 powder was immersed in 500 cm^3 of this mixed solution. After 20 d, the ion-exchanged specimen was filtered off without washing with water, and then dried in a desiccator for 1 d. A Li^+-extracted α-MnO_2 specimen was prepared by immersing the Li^+-inserted α-MnO_2 specimen in a mixed solution of 0.1 mol/dm^3 HNO_3 and 0.1 mol/dm^3 $LiNO_3$.

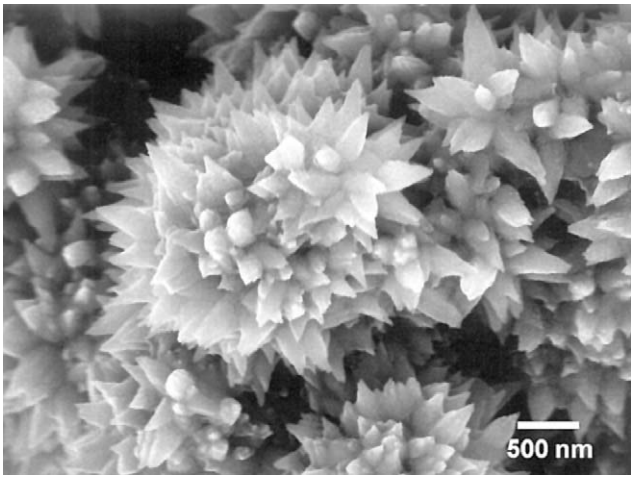

Fig. 2. Scanning electron microscopy image of an α-MnO_2 specimen.

Other conditions and procedures were the same as those of the lithium insertion.

2.2. Chemical analysis

The lithium and manganese contents were determined by inductively coupled plasma-atomic emission spectroscopy (ICP-AES). The experimental error of the ICP-AES measurements was within 4%. The water content in the specimen was measured by thermogravimetric (TG) method. Analytical values contain both adsorbed and tunnel water. The active oxygen content in each specimen was determined by the titration method recommended by Japan Industrial Standard [32]. The mean oxidation number of Mn, Z_{Mn}, was evaluated from the two analytical values using the formula

$$Z_{Mn} = 2 \times \left(1 + \frac{C(O_a)}{16} \times \frac{54.94}{C(Mn)}\right), \quad (1)$$

where $C(O_a)$ is the weight content of active oxygen in the specimen and $C(Mn)$ is the weight content of Mn in the specimen.

2.3. Ion-exchange property

pH titration curves were determined as follows. Mixed solutions of 0.1 mol/dm^3 HNO_3 + 0.1 mol/dm^3 $LiNO_3$ or 0.1 mol/dm^3 LiOH + 0.1 mol/dm^3 $LiNO_3$ in various ratios were prepared. The ionic strengths of these solutions were adjusted to 0.1 regardless of the ratios. Before immersing specimens in the solutions, the pH of each solution was measured with a pH meter as a blank test. Subsequently, 0.1 g of the specimen was immersed in 10 cm^3 of the solution with intermittent shaking at room temperature for 14 d. After attaining equilibrium, the pH of the supernatant solutions was measured.

Ion-exchange capacity was determined from changes in the Li concentration before and after the ion-exchange reactions. After equilibration, the supernatant solution was separated from the solid and analyzed for its Li concentration by ICP-AES. The concentration of Mn dissolved during the exchange process was below 0.5 wt% and could be neglected.

2.4. Electrochemical cell and measurements

Electrochemical insertion and extraction reactions were carried out using lithium cells. The working electrode consisted of 80 wt% active material, 15 wt% acetylene black (DENKA BLACK), and 5 wt% polytetrafluoroethylene powders. The mixture was pressed onto Al grids under a pressure 100 MPa. This electrode was dried at 120 °C for 1 d under vacuum and then moved to a glove box filled with Ar gas (−56 °C dew point) without exposure to air. The counter electrode was Li foil, and the separator was a microporous polypropylene sheet (SELGARD, #2400). The electrolyte was a 1 mol/dm^3 solution of $LiPF_6$ in blended ethylene carbonate (EC) and dimethyl carbonate (DMC) whose volumetric ratio was EC:DMC = 1:1. Cells used for electrochemical tests were constructed in a stainless-steel test cell (HS flat test cell, Hohsen Corp.). The cells were fabricated in an argon-filled glove box. Electrochemical measurements were carried out at room temperature after standing overnight on open-circuit potential. Galvanostatic charge–discharge cycles were performed with a Solartron 1287 potentiostat/galvanostat.

2.5. Structure analysis

X-ray powder diffraction (XRD) data were taken with Cu $K\alpha$ radiation at room temperature on a Bragg–Brentano-type powder diffractometer. The crushed specimen was loaded into a flat glass holder. The XRD data were measured in a 2θ range from 10° to 120° with a step interval of 0.03°.

The diffraction data were analyzed by the Rietveld method with RIETAN-2000 [33,34] on the basis of space group $I4/m$. A split pseudo-Voigt profile function formulated by Toraya [35] was used in all the refinements; the technique of partial profile relaxation [29,34] was applied to (nearly) isolated reflections, the profiles of which were anisotropically broadened. Table 1 lists other details in the Rietveld refinements.

The EDDs of specimens were visualized by MEM-based pattern fitting (MPF) [29–31]. After the Rietveld refinement, observed structure factors, F_o (Rietveld), were estimated from XRD data on the basis of refined parameters. The resulting F_o (Rietveld) data were analyzed by an MEM analysis program PRIMA [31]. In the subsequent w.p.f., structure factors were fixed at F_c (MEM)'s obtained by MEM analysis, while the scale factor and lattice, profile, peak-shift, and background parameters were refined by a least-squares method with RIETAN-2000. F_o(w.p.f.)'s reevaluated after the w.p.f. were analyzed again with PRIMA. The w.p.f. and MEM analysis were alternately repeated in the above way (REMEDY cycles) until R factors in the former no longer showed significant decreases. Three-dimensional EDD was visualized with VEND developed by Dilanian and Izumi [37].

3. Results and discussion

3.1. Structure analysis

A detailed structural analysis of the α-MnO_2 specimen has been reported in previous works [28]. In this paper, a Li^+-inserted α-MnO_2 specimen was analyzed. All of the

Table 1
Crystallographic data and details in the data collection and structure refinements [a]

Chemical formula	$(Li_2O)_{0.12}MnO_2$	
Crystal system	tetragonal	
Space group	$I4/m$	
Z	8	
a/Å	9.993(11)	
c/Å	2.853(3)	
V /Å^3	285.0(5)	
R_{wp}/%	7.17[b]	6.12[c]
R_e/%	3.61[b]	3.61[c]
R_p/%	5.66[b]	4.51[c]
R_B/%	3.90[b]	1.41[c]
R_F/%	1.31[b]	0.79[c]
S	1.98[b]	1.69[c]
Wavelength/Å	1.5418	
2θ range/°	10–120	
2θ step width/°	0.03	
Number of reflections	132	
Number of relaxed reflections	25	

[a]The R factors and S are defined in Ref. [36]. Numbers in parentheses give the estimated standard deviations of the last significant digit.
[b]After Rietveld refinement.
[c]After one REMEDY cycle.

reflections could be indexed on the basis of tetragonal symmetry with space group $I4/m$. Some of the reflections exhibited highly anisotropic profile broadening, stemming from stacking faults along the needle axis (Fig. 2). All of the $0\,0\,l$ reflections were sharp, but no systematic relations could be found among diffraction indices, $h\,k\,l$, and full-widths at half-maximum.

In preliminary analysis, EDD images detected significant scattering in the center of the tunnel space. This finding offers evidence for the existence of O atoms in the tunnel space because Li sites are practically transparent in the XRD experiment. Johnson et al. reported on a neutron diffraction analysis of a Li_2O-stabilized α-MnO_2 sample [11]. Their difference in the Fourier map resulting from a neutron diffraction data suggested that the O atom from the Li_2O molecule was located in the tunnel space. We therefore assigned the $2b(0,0,\frac{1}{2})$ site to a virtual chemical species, Li_2O, whose atomic scattering factor is the sum of those for one O and two Li atoms.

In the refinements, we ignored a small number of H_2O molecules occluded within the tunnel of α-MnO_2 because the chemical analysis indicated that Li_2O molecules fill the tunnel space almost entirely. Although a small amount of H^+ could also remain in the structure, H^+ sites were omitted because H^+ is transparent for X-rays. Therefore, the chemical formula of the Li^+-inserted α-MnO_2 specimen can be expressed as $(Li_2O)_{0.12}MnO_2$.

In the Rietveld refinements, thermal motion was regarded as an isotropic for all the sites, and $g(Li_2O)$ was fixed at the value anticipated from the chemical analysis because of a strong correlation between $U(Li_2O)$ and $g(Li_2O)$. After the refinement of an anisotropy coefficient for strain broadening, U_e, the technique of partial profile relaxation [29] was applied to 25 reflections. Despite the anisotropic profile broadening, partial profile relaxation improved the goodness-of-fit dramatically. For example, R_{wp} decreased from 12.05% to 7.17% as compared with the use of the pseudo-Voigt profile function of Thompson et al. [38], which was made asymmetric with the procedure of Finger et al. [39]. It should be noted that anisotropy coefficients for Scherrer broadening, X_e, and for strain broadening, Y_e, were also refined in the preliminary refinement using the above combination for representing profile shapes. Partial profile relaxation was most effective in the pattern fitting of our specimen because such porous materials often grow into needle crystals showing highly anisotropic profile broadening due to stacking faults along the needle axis. This kind of anisotropic profile broadening can hardly be expressed by profile functions with any physical meaning.

The resulting R factors reached $R_{wp} = 7.17\%$, $R_p = 5.66\%$, $R_B = 3.90\%$, and $R_F = 1.31\%$ with a goodness-of-fit indicator of $S = R_{wp}/R_e = 1.98$. Fig. 3 shows the observed, calculated, and difference patterns for the Rietveld refinement from the XRD data of $(Li_2O)_{0.12}MnO_2$. Lattice parameters were $a = 9.993(11)$ and $c = 2.853(3)$ Å. Tables 2 and 3 list the structure parameters of $(Li_2O)_{0.12}MnO_2$, and selected interatomic distances and bond angles, respectively.

The Rietveld refinements were followed by MPF to determine EDD. After one REMEDY cycle, R factors decreased to $R_{wp} = 6.12\%$, $R_p = 4.51\%$, $R_B = 1.41\%$, and $R_F = 0.79\%$ with $S = 1.69$. The dramatic decreases in R_B and R_F evaluated from the observed integrated intensities are particularly noteworthy, reflecting a better representation of crystal structures with three-dimensional electron densities in MPF than with

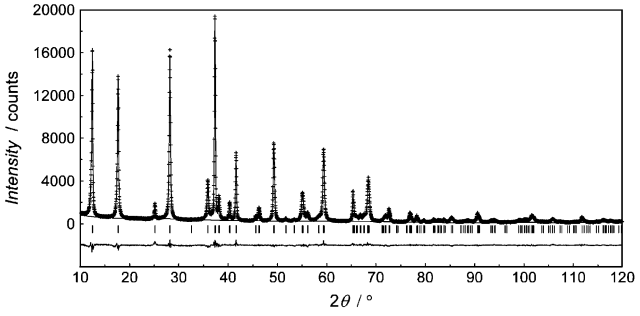

Fig. 3. Observed (plus marks), calculated (solid line), and difference (bottom) patterns for the Rietveld refinement from the X-ray diffraction data of $(Li_2O)_{0.12}MnO_2$. The short vertical lines below the profiles mark the peak positions of all the possible Bragg reflections.

Table 2
Structure parameters of $(Li_2O)_{0.12}MnO_2$ determined from the XRD data[a]

Atom	Site	g	n	x	y	z	$U/Å^2$
Mn	8*h*	1	8	0.34936(14)	0.1659(2)	0	0.0036(3)
O1	8*h*	1	8	0.1472(4)	0.1988(3)	0	0.0049(8)
O2	8*h*	1	8	0.5394(4)	0.1681(4)	0	$= U$(O1)
Li_2O	2*b*	0.48	0.96	0	0	$\frac{1}{2}$	0.012(3)

[a] *Definitions*: g, occupation factor; n, number of atoms per unit cell. U is the isotropic atomic displacement parameter when the Debye–Waller factor is represented as $\exp(-8\pi^2 U \sin^2\theta/\lambda^2)$.

Table 3
Selected interatomic distances, l, and bond angles, ϕ, calculated from the crystal data obtained with the XRD data of $(Li_2O)_{0.12}MnO_2$[a]

$l/Å$	
Mn–O1	2.046(4)
Mn–O1$^{(i)}$ × 2	1.965(3)
Mn–O2	1.899(4)
Mn–O2$^{(ii)}$ × 2	1.914(3)
Mean	1.9505
$\phi/^\circ$	
O1–Mn–O1$^{(i)}$	84.64(14)
O1–Mn–O2$^{(ii)}$	90.9(2)
O1$^{(i)}$–Mn–O2	88.5(2)
O1$^{(i)}$–Mn–O2$^{(ii)}$	85.09(13)
O2–Mn–O2$^{(ii)}$	95.6(2)

[a] *Symmetry codes*: (i) $\frac{1}{2}-x, \frac{1}{2}-y, \frac{1}{2}-z$; (ii) $\frac{1}{2}-y, -\frac{1}{2}+x, \frac{1}{2}+z$.

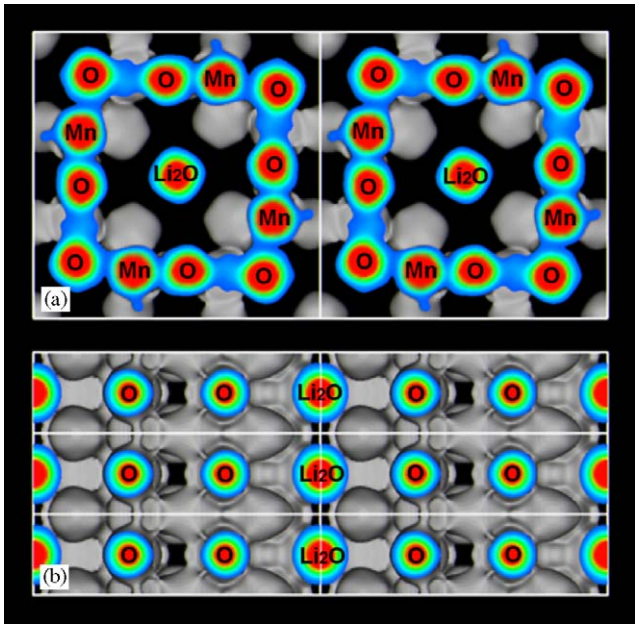

Fig. 4. Three-dimensional EDD images viewed along the (a) [001] and (b) [100] directions for $(Li_2O)_{0.12}MnO_2$. The equi-density level was $0.3/Å^3$. The solid boxes indicate the unit cell.

structure parameters in the Rietveld analysis. Fig. 4 depicts the three-dimensional EDD images of $(Li_2O)_{0.12}MnO_2$ obtained by MPF.

3.2. Ion exchange properties

Table 4 lists the compositional and structural parameters of original, Li^+-inserted, and Li^+-extracted α-MnO_2 specimens. Considerable differences were discovered among their lattice parameters. Lattice parameters were very sensitive to the Li content. As the amount of Li content increased, a increased while c hardly changed. This tendency is consistent with those reported in the literature [11]. On the other hand, Z_{Mn} decreased slightly regardless of the amount of Li content whenever ions were exchanged.

Table 5 gives the Li/Mn molar ratio and ion-exchange capacity of original, Li^+-inserted, and Li^+-extracted α-MnO_2 specimens. The ion-exchange capacity of our original α-MnO_2 specimen reached 3.25 meq/g, which is higher than the 2.48 meq/g value reached by K^+-extracted HMO (KHMO) [23]. The Li/Mn molar ratio of the Li^+-inserted specimen showed that about two Li^+ ions can be inserted into one unit cell of the hollandite-type structure.

As Table 5 lists, the Li^+-extraction capacity of the Li^+-inserted α-MnO_2 specimen was smaller than the Li^+-insertion capacity of the parent α-MnO_2 specimen. This fact shows that all of the inserted Li^+ ions could not be extracted from the structure, and that some Li^+ ions remained in the structure. Furthermore, the number of Li^+ ions that can be inserted into the structure increased slightly whenever ions were exchanged because the Li^+-insertion capacity of the Li^+-extracted α-MnO_2 specimen was larger than the Li^+-extraction capacity of the Li^+-inserted one.

Fig. 5 shows the pH titration curves for original, Li^+-inserted, and Li^+-extracted α-MnO_2 specimens. The pH titration curve of our α-MnO_2 specimen showed a monobasic acid behavior toward Li^+. The ion-exchange characteristic of a HMO seems to depend on a synthetic route. KHMO indicated a dibasic acid

Table 4
Compositional and structural parameters of original, Li^+-inserted, and Li^+-extracted α-MnO_2 specimens

Sample	Weight contents (%)					Lattice constants (Å)	
	Z_{Mn}	Li	Mn	O_a	H_2O[a]	*a*	*c*
Original sample	3.98	0	58.7	16.9	6.9	9.805(4)	2.8510(13)
Li^+-inserted sample	3.94	1.7	56.5	16.0	7.3	9.993(11)	2.853(3)
Li^+-extracted sample	3.91	0.2	59.2	16.5	6.2	9.844(4)	2.8569(11)

[a]TG weight losses below 400 °C.

Table 5
Li/Mn molar ratio, ion-exchange capacity, and first discharge capacity of original, Li^+-inserted, and Li^+-extracted α-MnO_2 specimens

Sample	Molar ratio (Li/Mn)	Ion-exchange capacity (meq/g)	First discharge capacity[a] (mAh/g)
Original sample	0	3.25 (Li^+ insertion)	65 (Li/Mn = 0.21)[b]
Li^+-inserted sample	0.24	2.18 (Li^+ extraction)	230 (Li/Mn = 0.79)[b]
Li^+-extracted sample	0.03	2.67 (Li^+ re-insertion)	214 (Li/Mn = 0.73)[b]

[a]Cut off voltage is 1.6 V.
[b]Calculated from the first discharge capacity.

behavior [20,21,23,26] while the H^+-form HMO (HHMO) showed a monobasic acid behavior [4,24,25]. The present pH titration curves are different from those in the case of KHMO but consistent with those of HHMO.

The ion-exchange mechanism for the HMO has been the subject of controversy. Feng et al. have proposed that alkali metal ions can be inserted or extracted by both redox-type and ion-exchange-type reactions [4,24,25]. They described these reactions as follows:

$$(\square)[Mn_8^{4+}]O_{16} + 2LiOH \rightarrow (Li_2^+)[Mn_2^{3+}Mn_6^{4+}]O_{16} + H_2O + (1/2)O_2, \quad (2)$$

$$8(Li_2^+)[Mn_2^{3+}Mn_6^{4+}]O_{16} + 32H^+ \rightarrow 7(\square)[Mn_8^{4+}]O_{16} + 16Li^+ + 8Mn^{2+} + 16H_2O \quad (3)$$

for the redox reaction;

$$(H_2^+)[\square_{0.5}Mn_{7.5}^{4+}]O_{16} + 2Li^+ \rightleftharpoons (Li_2^+)[\square_{0.5}Mn_{7.5}^{4+}]O_{16} + 2H^+ \quad (4)$$

for the ion-exchange reaction, where ( ) denotes (2 × 2) tunnel sites, [ ] octahedral sites occupied by Mn, and □ vacant sites. On the other hand, Tanaka et al. have claimed that no redox process is associated with the cation exchange [26]. They reported that no evidence of reduction to lower valent Mn ions was detected by X-ray photoelectron spectroscopy spectra.

We recently reported a neutron diffraction study of a partially deuterated specimen of $MnO_2 \cdot 0.1(D_{0.34}H_{0.66})_2O$ [28]. There was no possibility of the existence of Mn^{3+} ions and Mn vacancies in our α-MnO_2 specimen, and an attempt to determine the position of the proton site responsible for ion-exchange was unsuccessful.

The redox-type reaction would not be dominant in our specimen because the change of Z_{Mn} between our parent and Li^+-inserted α-MnO_2 specimens is smaller than that in the case of HHMO [24]. The EDD images demonstrate that our parent α-MnO_2 specimen has residual H_2O molecules in the tunnel space [28], and the EDD images of the Li^+-inserted α-MnO_2 specimen show that Li_2O molecules exist in the tunnel space, as Fig. 2 depicts. Although small amounts of Mn^{3+} ions and Mn defects would be generated by the ion-exchanges, most H_2O molecules in the tunnel space seem to be simply replaced by Li_2O molecules. The tentative reaction can be described as follows:

$$(H_2O)[Mn_8^{4+}]O_{16} + 2LiOH \rightarrow (Li_2O)[Mn_8^{4+}]O_{16} + 2H_2O. \quad (5)$$

Johnson et al. reported that valence state of Mn in a Li_2O-stabilized α-MnO_2 sample was almost tetravalent [11], which is consistent with our results. The Li_2O molecules might be inserted by other mechanisms besides the redox and ion-exchange reactions.

3.3. Electrochemical performances

Fig. 6 shows the first charge–discharge curves of original, Li^+-inserted, and Li^+-extracted α-MnO_2 specimens. The open-circuit voltages were 3.36 V for the original specimen, 3.65 V for the Li^+-inserted specimen, and 3.60 V for the Li^+-extracted specimen, respectively. To extract the ion-exchanged Li^+ ions from the

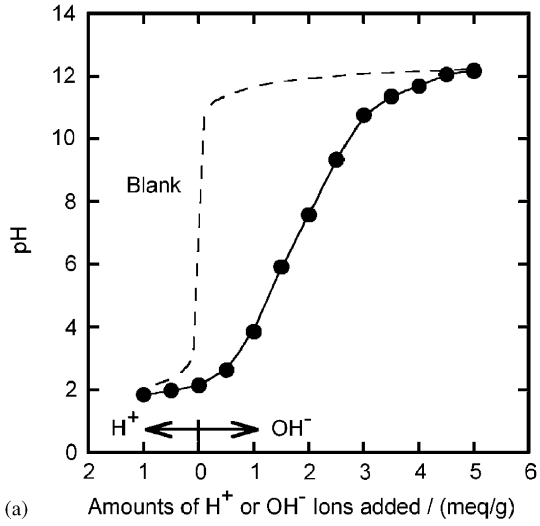

(a)

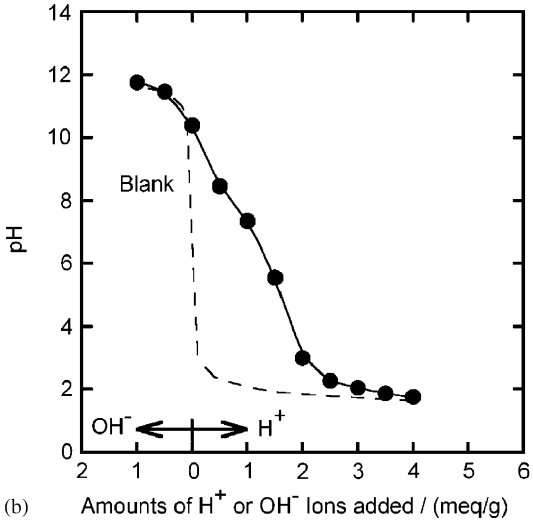

(b)

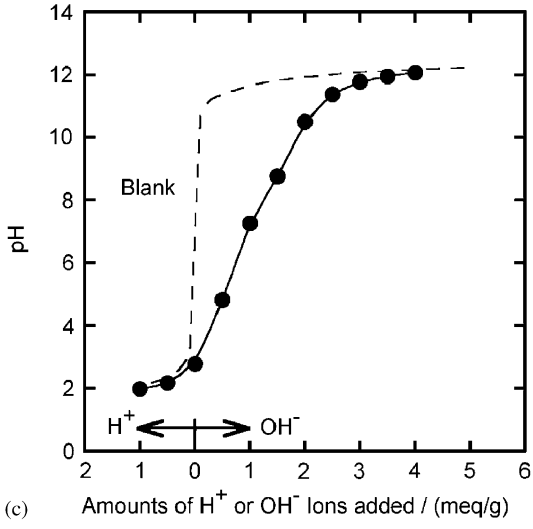

(c)

Fig. 5. pH titration curves for (a) original, (b) Li^+-inserted, and (c) Li^+-extracted α-MnO_2 specimens: sample, 0.1 g; solution, 0.1 mol/dm^3 $LiNO_3 + LiOH$ or 0.1 mol/dm^3 $HNO_3 + LiNO_3$; total volume of solution, 10 cm^3. The broken lines show blank titrations.

structure, the ion-exchanged specimens were charged before first discharging.

The parent α-MnO_2 specimen gave a poor discharge property, as Fig. 6a shows. In contrast, the Li^+-inserted α-MnO_2 specimen showed a good charge–discharge property as the cathode, as Fig. 6b displays. A high potential (>3.6 V) was required during the first charge to extract the ion-exchanged Li^+ ions, and all Li^+ ions could be extracted at the initial charge. A subsequent discharge capacity of approximately 230 mAh/g could be achieved, and this discharge capacity showed that about six Li^+ ions can be inserted into one unit cell of the hollandite-type structure. More Li^+ ions can be inserted electrochemically as compared with the ion-exchange method. Fig. 6c demonstrates that the charge–discharge property of the Li^+-extracted α-MnO_2 specimen was slightly inferior to the Li^+-inserted specimen but better than that of the parent specimen. The charge–discharge performance was improved significantly after the lithium insertion/extraction reactions.

The hollandite-type structure has a (2×2) tunnel and the rutile-type a (1×1) linkage, as Fig. 1 shows. Li^+ ions can be inserted only into the (2×2) tunnels because β-MnO_2 having (1×1) tunnels proves inactive to both electrochemical and chemical lithium intercalation [40,41]. Johnson et al. reported a preliminary neutron diffraction study of a Li_2O-stabilized α-MnO_2 sample [11]. Although a refinement of the structure parameters was not performed, their difference Fourier map indicated that the Li^+ ions were located at $(0.204, 0.078, 0.0)$ in the (2×2) tunnel. In future work, such a Li site should be decided by neutron diffraction.

Fig. 7 shows the charge–discharge curves and evolution of discharge capacity for the Li^+-inserted specimen over the first 10 cycles. The specimen was charged before the first discharge. The first discharge capacity exceeded 200 mAh/g, and the reaction was reversible, whereas a capacity was lost steadily on cycling. The first discharge profile was characterized by some independent (slightly sloping) voltage plateaus. With cycling, however, the plateaus disappeared and the discharge adopted a single sloping profile, typical of a single-phase insertion electrode. This tendency is consistent with that of the charge–discharge properties of a Li_2O-stabilized α-MnO_2 sample [11]. An X-ray diffraction study of the used electrode indicated that there was no damage to the framework structure of α-MnO_2 after the charge–discharge cycling test because almost all of the possible Bragg reflections were observed and no extra peaks were detected. The capacity loss would be related to a modification of local structure, especially that in the tunnel space.

In our synthetic method, α-MnO_2 can directly be formed in solutions containing no cations other than Mn^{2+} [27,28]. Therefore, our α-MnO_2 specimen does not

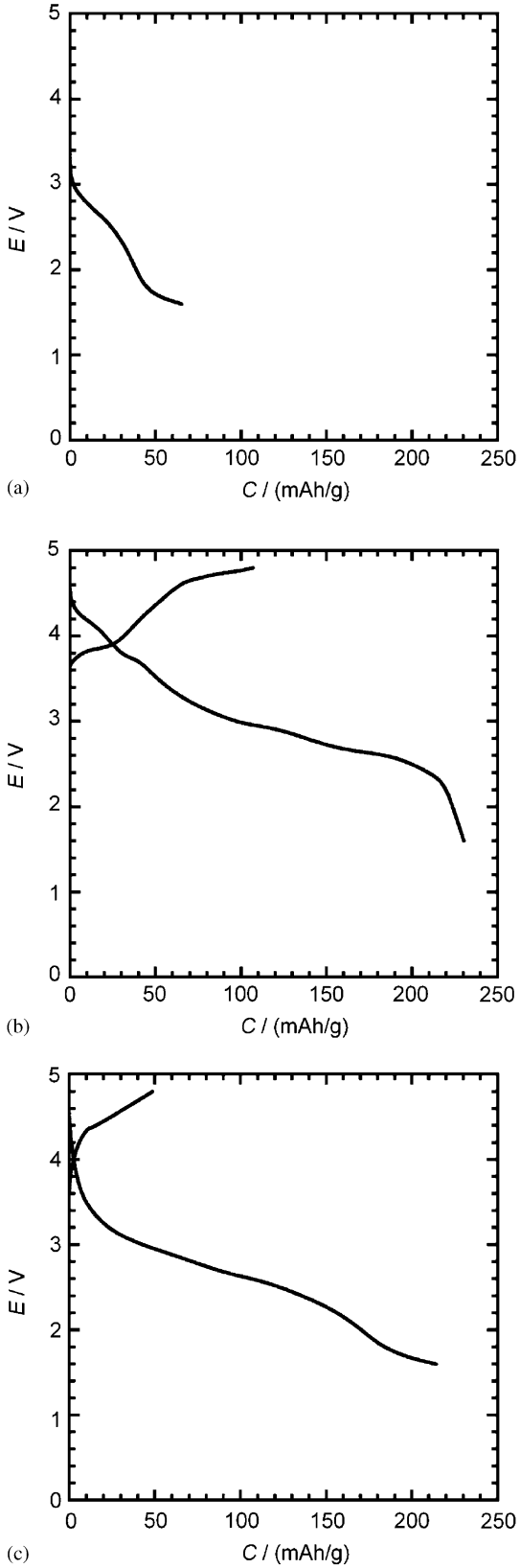

Fig. 6. First charge–discharge curves for (a) original, (b) Li^+-inserted, and (c) Li^+-extracted α-MnO_2 specimens with a current rate of 10 mA/g. The ion-exchanged specimens were charged before first discharging.

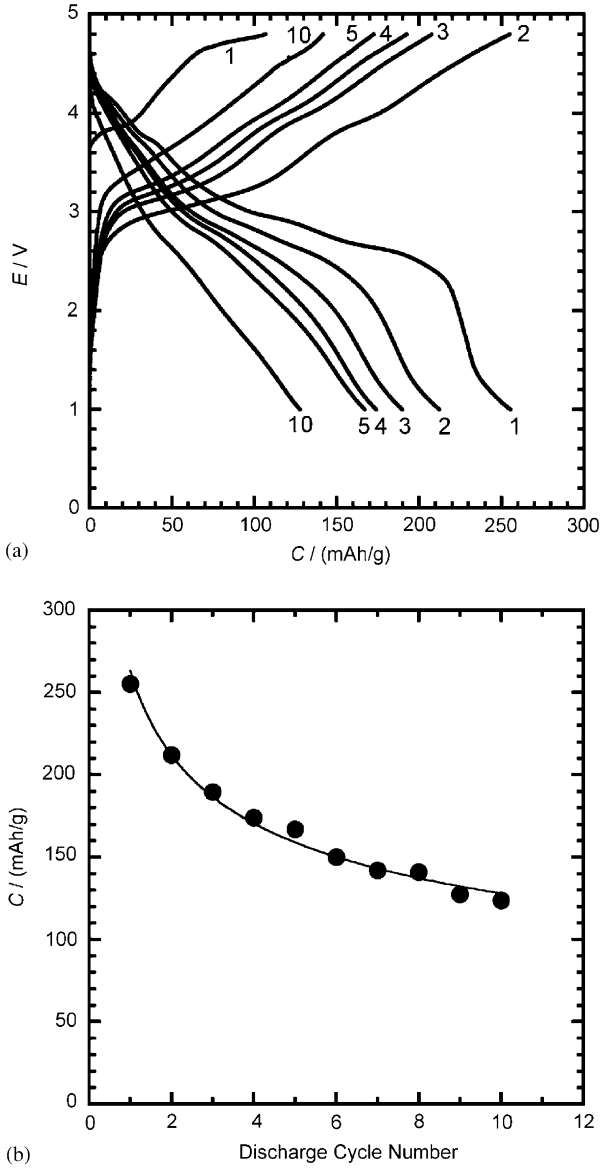

Fig. 7. (a) Charge–discharge curves and (b) evolution of discharge capacity for $(Li_2O)_{0.12}MnO_2$ over the first 10 cycles; voltage: 4.8–1.0 V, and current rate: 10 mA/g.

contain any cationic residues such as Li^+, K^+, and Ba^{2+} ions in the tunnels. Furthermore, the inside of the tunnel cavity is absolutely empty because residual H_2O molecules were removed from the tunnel space before the cell construction. The stabilizing cations in the hollandite-type structure have for a long time been believed to impede the diffusion of Li^+ ions in the tunnels during electrochemical operation. Our parent α-MnO_2 specimen, however, showed a poor discharge property despite the fact that no cationic residues or molecules remained in the tunnel space.

In contrast, the Li^+-inserted α-MnO_2 specimen exhibited a good charge–discharge property. As Fig. 2

depicts, the EDD images of the Li^+-inserted α-MnO_2 specimen show that Li_2O molecules almost fill the tunnel space. Ohzuku et al. have reported on the charge–discharge properties of hollandite-type $K_{1.3}Mn_8O_{16}$ and $Rb_{1.3}Mn_8O_{16}$ compounds [6]. Although their electrochemical performances are inferior to our Li^+-inserted α-MnO_2 specimen, they are better than that of our α-MnO_2 specimen with empty tunnels. These facts suggest that the presence of stabilizing atoms or molecules within the (2×2) tunnel of a hollandite-type structure is necessary to facilitate the diffusion of Li^+ ions during charge–discharge cycling.

Finally, we point out the possibility of improving the battery performance with HMO. Johnson et al. have reported that a combination of Li_2O doping and NH_3 treatment of the active material powder having the composition $[(Li_2O)_{0.143}(HN_3)_{0.007}]MnO_2$ gave the best electrochemical performance [17]. One task for future research is to find other stabilizing atoms or molecules that enhance the electrochemical performance.

4. Summary

1. The pH titration curve of the α-MnO_2 specimen showed a monobasic acid behavior toward Li^+, and an ion-exchange capacity of 3.25 meq/g was reached at $pH > 11$. As the amount of Li content was increased, the lattice parameter a increased while c hardly changed. On the other hand, the mean oxidation number of Mn decreased slightly regardless of the amount of Li content whenever ions were exchanged.
2. The Li^+-inserted α-MnO_2 specimen reduced topotactically in one phase when it was used as an active cathode material in a liquid organic electrolyte lithium cell. An initial discharge capacity of approximately 230 mAh/g could be achieved, and the reaction was reversible, but this capacity decreased steadily upon cycling.
3. The Li/Mn molar ratio of the Li^+-inserted α-MnO_2 specimen showed that about two Li^+ ions can be chemically inserted into one unit cell of the hollandite-type structure. On the other hand, about six Li^+ ions can be electrochemically inserted.
4. The structure parameters of the Li^+-inserted specimen of $(Li_2O)_{0.12}MnO_2$ were determined by Rietveld refinement of XRD data, and the EDD images in $(Li_2O)_{0.12}MnO_2$ were visualized by MPF. The EDD images in $(Li_2O)_{0.12}MnO_2$ showed that the Li_2O molecules almost fill the tunnel space.
5. The parent α-MnO_2 specimen showed a poor discharge property although no cationic residues or residual H_2O molecules remained in the tunnel space. In contrast, the Li^+-inserted α-MnO_2 specimen showed a good charge–discharge property as the cathode. These facts suggest that the presence of stabilizing atoms or molecules within the (2×2) tunnel of a hollandite-type structure is necessary to facilitate the diffusion of Li^+ ions during cycling.

Acknowledgement

We would like to thank Dr. M. Tabuchi at AIST for his technical advice about electrochemical measurements.

References

[1] A.F. Wells, Structural Inorganic Chemistry, fifth ed., Clarendon Press, Oxford, 1984, pp. 555–556.
[2] M.M. Thackeray, Prog. Solid State Chem. 25 (1997) 1–71 and references therein.
[3] S.L. Brock, N. Duan, Z.R. Tian, O. Giraldo, H. Zhou, S.L. Suib, Chem. Mater. 10 (1998) 2619–2628 and references therein.
[4] Q. Feng, H. Kanoh, K. Ooi, J. Mater. Chem. 9 (1999) 319–333 and references therein.
[5] J.E. Post, Proc. Natl. Acad. Sci. USA 96 (1999) 3447–3454 and references therein.
[6] T. Ohzuku, M. Kitagawa, K. Sawai, T. Hirai, J. Electrochem. Soc. 138 (1991) 360–365.
[7] M.H. Rossouw, D.C. Liles, M.M. Thackeray, Mater. Res. Bull. 27 (1992) 221–230.
[8] M.A. Humbert, P. Biensan, M. Broussely, A. Lecerf, A. Dollé, H. Ladhily, J. Power Sources 43–44 (1993) 681–687.
[9] S. Bach, J.P. Pereira-Ramos, N. Baffier, Solid State Ionics 80 (1995) 151–158.
[10] M.H. Rossouw, D.C. Liles, M.M. Thackeray, Prog. Batteries Battery Mater. 15 (1996) 8–18.
[11] C.S. Johnson, D.W. Dees, M.F. Mansuetto, M.M. Thackeray, D.R. Vissers, D. Argyriou, C.-K. Loong, L. Christensen, J. Power Sources 68 (1997) 570–577;
Erratum, J. Power Sources 75 (1998) 183–184.
[12] C.S. Johnson, M.F. Mansuetto, M.M. Thackeray, Y. Shao-Horn, S.A. Hackney, J. Electrochem. Soc. 144 (1997) 2279–2283.
[13] Q. Feng, H. Kanoh, K. Ooi, M. Tani, Y. Nakacho, J. Electrochem. Soc. 141 (1994) L135–L136.
[14] Y. Shao-Horn, S.A. Hackney, C.S. Johnson, M.M. Thackeray, J. Electrochem. Soc. 145 (1998) 582–589.
[15] J. Dai, S.F.Y. Li, K.S. Siow, Z. Gao, Electrochim. Acta 45 (2000) 2211–2217.
[16] S. Barbato, J.L. Gautier, Electrochim. Acta 46 (2001) 2767–2776.
[17] C.S. Johnson, M.M. Thackeray, J. Power Sources 97–98 (2001) 437–442.
[18] M. Sugantha, P.A. Ramakrishnan, A.M. Hermann, C.P. Warmsingh, D.S. Ginley, Int. J. Hydrogen Energy 28 (2003) 597–600.
[19] T. Sasaki, N. Kumagai, S. Komaba, H. Yashiro, Electrochemistry 72 (2004) 688–693 (in Japanese).
[20] M. Tsuji, M. Abe, Solvent Extraction Ion Exchange 2 (1984) 253–274.
[21] M. Tsuji, M. Abe, Bull. Chem. Soc. Jpn. 58 (1985) 1109–1114.
[22] A. Clearfield, Chem. Rev. 88 (1988) 125–148 and references therein.
[23] M. Tsuji, S. Komarneni, J. Mater. Res. 8 (1993) 3145–3150.
[24] Q. Feng, H. Kanoh, Y. Miyai, K. Ooi, Chem. Mater. 7 (1995) 148–153.
[25] Q. Feng, H. Kanoh, K. Ooi, J. Ion Exchange 8 (1997) 102–114 (in Japanese).

[26] Y. Tanaka, M. Tsuji, Y. Tamaura, Phys. Chem. Chem. Phys. 2 (2000) 1473–1479.
[27] N. Kijima, H. Yasuda, T. Sato, Y. Yoshimura, J. Solid State Chem. 159 (2001) 94–102;
Erratum, J. Solid State Chem. 160 (2001) 292.
[28] N. Kijima, T. Ikeda, K. Oikawa, F. Izumi, Y. Yoshimura, J. Solid State Chem. 177 (2004) 1258–1267.
[29] F. Izumi, Rigaku J. 17 (2000) 34–45.
[30] F. Izumi, S. Kumazawa, T. Ikeda, W.-Z. Hu, A. Yamamoto, K. Oikawa, Mater. Sci. Forum 378–381 (2001) 59–64.
[31] F. Izumi, R.A. Dilanian, Recent Research Developments in Physics, vol. 3, Transworld Research Network, Trivandrum, 2002, pp. 699–726.
[32] Japan Industrial Standard (JIS), 1995, M8233–1995, Manganese ores—Methods for determination of active oxygen content.
[33] F. Izumi, in: R.A. Young (Ed.), The Rietveld Method, Oxford University Press, Oxford, 1995 (Chapter 13).
[34] F. Izumi, T. Ikeda, Mater. Sci. Forum 321–324 (2000) 198–203.
[35] H. Toraya, J. Appl. Crystallogr. 23 (1990) 485–491.
[36] R.A. Young, in: R.A. Young (Ed.), The Rietveld Method, Oxford University Press, Oxford, 1995 (Chapter 1).
[37] R.A. Dilanian, F. Izumi, Unpublished Work.
[38] P. Thompson, D.E. Cox, J.B. Hastings, J. Appl. Crystallogr. 20 (1987) 79–83.
[39] L.W. Finger, D.E. Cox, A.P. Jephcoat, J. Appl. Crystallogr. 27 (1994) 892–900.
[40] D.W. Murphy, F.J. DiSalvo, J.N. Carides, J.V. Waszczak, Mater. Res. Bull. 13 (1978) 1395–1402.
[41] W. Wang, M. Wu, X. Liu, J. Solid State Chem. 164 (2002) 5–11.